

ALGORITHM OF SPACE RESECTION AND ITS EVALUATION

Nobuo MAKIMOTO †

Jun-ichi TAGUCHI †

† Systems Development Laboratory, Hitachi Ltd., Kawasaki, Japan

Commission V, Working Group 1

KEYWORDS: SPACE RESECTION, ORIENTATION, SATELLITE IMAGE PROCESSING, COMPUTER VISION, NONLINEAR OPTIMIZATION, NUMERICAL ANALYSIS

ABSTRACT

Space resection is a technique for calibrating camera parameters, mainly the angle and the position, by looking at the images of GCPs (points on the ground with known position) on a picture taken by the camera and is an indispensable technique in the field of satellite image processing. In this paper we describe a new algorithm for space resection. First, and most important, we derive space resection equations in a new form. Specifically, we split the least-square equation into two parts by square completion: one is an equation only of the angle; the other is an explicit formula to calculate the position directly from the angle. We also derive formulae for the variances of the errors of the least-square estimators. We also describe a method for numerical solution of the angle equation. The difficulty is that the equation has a few tens of fake solutions. To find the true solution (global minimum) among these fake solutions, we propose some techniques of nonlinear optimization. Evaluation of the proposed method by computer simulation shows that the global minimum is obtained efficiently when four or more GCPs are available. The simulation results also show that the variance formulae are valid, and this means we can guarantee the precision of the estimated camera parameters. The proposed optimization techniques are applicable to a wide range of nonlinear optimization problems other than space resection.

1 INTRODUCTION

1.1 Background and Summary

Space resection, a technique for finding the angle and the position of a camera from a picture taken by it, is indispensable in the field of satellite image processing.

It is usually formulated as a nonlinear least-squares estimation, but is not easy to solve because of its search space is large and there is a large number of local minima. In this paper we focus on the following aspects of space resection (though some are in the appendix).

- New equations:
We split the conventional equation into two small parts by some elementary linear algebra.
- Numerical solution:
We propose "absolute Newton method" and some other techniques of nonlinear optimization.

- Error analysis:

We derive practical variance formulae and prove the approximate efficiency of the estimator.

A numerical simulation shows that the proposed numerical solution is very stable and that we can guarantee the precision of the estimator by the variance formulae.

1.2 The Problem of Space Resection

First let us introduce some notations. The camera model is illustrated in Fig.1. X_0 is the position, or the viewpoint, of the camera. The orthonormal frame $R = (e_1, e_2, e_3)$ represents the orientation of the camera. The image plane is spanned by e_2, e_3 and is separated from X_0 by the focal length c . A GCP (ground control point) is a point on the ground whose position (latitude, longitude, and height) is known in advance. Each GCP X_i is imaged onto the point x_i on the plane by the central projection with its center X_0 .

The variances of the measurement error of X_i and x_i are respectively P and Q .

§A.1 and considering the coordinate transformation R , we can write the condition as

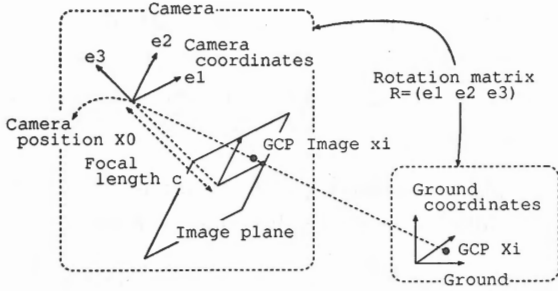


Fig. 1: Camera model.

With this notation, the main problem in this paper can be described as follows:

Given a set of GCP data $\{X_i, x_i\} (i = 1, 2, \dots)$, find the position X_0 and the orientation R of the camera.

We assume that the values of c , P , and Q are known. See §A.1 for more detail on the notation.

2 NEW EQUATIONS

In this section we derive new equations of space resection. The outline of the argument is as follows. We represent the collinearity condition as an orthogonality condition (1) rather than as the conventional parallelism condition so that the square-error function (2) becomes a quadratic form of X_0 . By square completion with respect to X_0 , the least-square equation splits into two parts: (5) and (6).

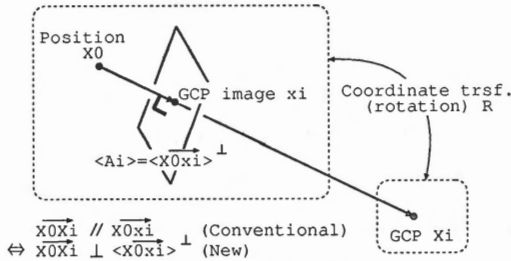


Fig. 2: Collinearity condition.

The collinearity condition states that the direction from the viewpoint to a GCP X_0X_i and to its image X_0x_i coincide, or equivalently, X_0X_i and the orthogonal complement $\langle X_0x_i \rangle^\perp$ are orthogonal (Fig. 2). Thus letting A_i be a basis of $\langle X_0x_i \rangle^\perp$ as described in

$$(R(\theta)A_i)' \cdot (X_i - X_0) = 0. \quad (1)$$

In general, because of errors the left-hand side of (1) does not vanish. So we consider the following square-error function:

$$\begin{aligned} e_0(\theta, X_0) &= \sum_{i: \text{GCP}} \{\text{LHS of (1)}\}' S_i^{-1} \{\text{LHS of (1)}\} \\ &= X_0' B X_0 - 2 C' X_0 + D, \end{aligned} \quad (2)$$

where

$$\begin{aligned} B &= \sum_i (A_i R)' S_i^{-1} (A_i R) \\ C &= \sum_i (A_i R)' S_i^{-1} (A_i R X_i) \\ D &= \sum_i (A_i R X_i)' S_i^{-1} (A_i R X_i) \end{aligned}$$

and S_i is a given weight for the i -th GCP (here we simply set this weight to be the unit matrix; also see §A.2.4).

Since B is clearly positive definite in generic cases, we can deform the quadratic form (2) by square completion as $e_0 = \|B^{1/2}X_0 - B^{-1/2}C\|^2 + D - C'B^{-1}C$. The minimizing X_0 is $B^{-1}C$, regardless of $R = R(\theta)$. Therefore if we define

$$e(\theta; \{X_i, x_i\}) = D - C'B^{-1}C \quad (3)$$

$$h(\theta; \{X_i, x_i\}) = B^{-1}C, \quad (4)$$

the least-square equation splits into two parts:

$$\frac{\partial e}{\partial \theta}(\theta) = 0 \quad (5)$$

$$X_0 = h(\theta) \quad (6)$$

Equation (5) is an equation only of the angle θ and (6) is an explicit formula of the position X_0 . The new

equation (5) is expected to be much easier to solve than the conventional one [Fu et al., 1987] because its search space is homogeneous and much smaller than that of the conventional one.

3 NUMERICAL SOLUTION

In this section we propose a numerical solution to find the desired solution of (5), the global minimum of the square-error function (3). In §3.1 we describe the outline of the procedure, and in §3.2 and §3.3 we describe and justify some techniques involved: “potential addition” and the “absolute Newton method.” See §A.2 for other techniques and analysis.

3.1 Outline

Fig. 3 shows the flow of the procedures: minimal points are found one after another and then the most desirable one is selected.

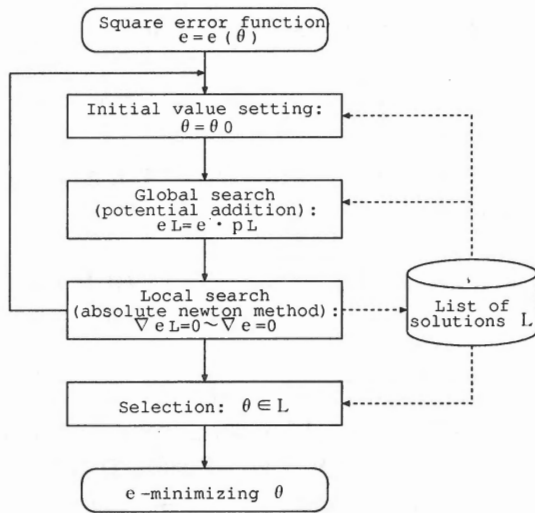


Fig. 3: Flow of numerical solution.

We choose the initial value of iterative method efficiently, according to some geometric considerations (§A.2.1), and then we add a “potential term” to the square-error function. It plays a role of a “repulsive force” against already-found solutions, and thus we can find different solutions (§3.2). We then search for a minimal point of e by using a modified Newton method that converges to a minimal point of e , not to a saddle or maximal point (§3.3). The minimal point thus found is added to the list of solutions L . By repeating the above 3 steps we can list up major minimal points. Finally we select the global minimum from the list L .

3.2 Global Search – Potential Addition

To find the global minimum of the square-error function, we propose a simple method of “potential addition.” The idea is very similar to that of the “Tunneling Algorithm” [Levy et al., 1985], though the implementation is slightly different. The procedure is as follows:

1. Apply local search (as described in §3.3) to the modified square error function e_L below.
2. Apply local search again to e , this time with the initial value equal to the result of step 1.
3. Add the result of step 2 to the list L .

The modified square-error function e_L is defined as

$$e_L(\theta) = e(\theta) \cdot p_L(\theta)$$

$$p_L(\theta) = 1 + \sum_{\theta_k \in L} AB \left\| \frac{1}{B}(\theta - \theta_k) \right\|^2,$$

where L is the list of minimal points of e already found and where A and B are respectively an appropriate weight and scale factor. p_L has poles at points $\in L$.

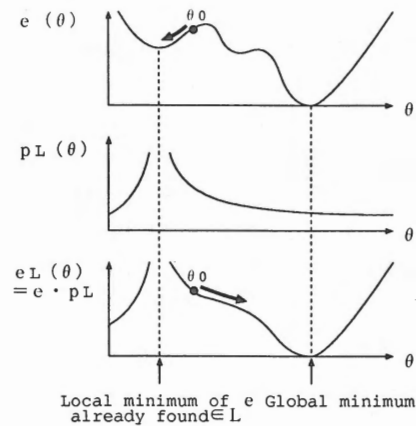


Fig. 4: Potential addition.

With the above procedure we can find a minimal point other than that of L in Fig. 3, as explained below (Fig. 4). In a neighborhood of L , e_L has no minimal point because p_L grows rapidly. In a region away from L , on the other hand, the minimal points of e and e_L are close to each other because there p_L is nearly constant. If $\theta \notin L$ is the global minimum of e , it is almost the global minimum of e_L as well (and vice versa), since the values of nonnegative functions e and e_L are both approximately 0 at θ .

p_L plays the role of a potential field and is thus a source of “repulsive force” against L . One of the advantages of the above procedure is that it is deterministic.

3.3 Local Search – Absolute Newton Method

To find a local minimum of a given smooth function $f = f(\theta)$, we propose an “absolute” Newton method. It is just the Newton method [Kahaner et al., 1989] applied to ∇f , with the Hessian replaced by its absolute value in the recurrence formula:

$$\theta_{n+1} = \theta_n - |Hf(\theta_n)|^{-1} \nabla f(\theta_n), \quad (7)$$

where $Hf = (\partial_i \partial_j f)$ is the Hessian of the function f and where $|\cdot|$ stands for the absolute value of a symmetric transformation (i.e., each eigenvalue is the absolute value of eigenvalue of the operand).

By using the recurrence formula (7), we can search for only the minimal points among all the solutions of $\nabla f = 0$. Actually, it is easy to see that the only stable fixed points of (7) are the solutions of $\nabla f = 0$ with positive definite Hessian (i.e., the minimal points), while the ordinary Newton method [Kahaner et al., 1989] has all the (nondegenerate) solutions of $\nabla f = 0$ as its stable fixed points. Near a minimal point the results of the absolute Newton method coincides with the ordinary Newton method, so it converges rapidly. See §A.2.2 for related arguments.

4 VARIANCE FORMULAE

In this section we derive formula for the variance of the least-square estimator. See also §A.2.4 for some properties of the estimator. There are some errors in the observed values of the GCP data $\{X_i, x_i\}$ and the estimated values of the camera angle θ . We denote their true values by X_i^0, x_i^0, θ^0 and their errors by $\Delta X_i = X_i - X_i^0$, $\Delta x_i = x_i - x_i^0$, $\Delta \theta = \theta - \theta^0$.

Both the true values $\{\{X_i^0, x_i^0\}, \theta^0\}$ and the observed/estimated values $\{\{X_i, x_i\}, \theta\}$ satisfy equation (5). Thus, considering the Taylor expansion of the gradient of the square-error function $g(\theta; \{X_i, x_i\}) = \nabla e$ and ignoring the higher-order terms, we can write

$$\frac{\partial g}{\partial \theta} \Delta \theta + \sum_i \left\{ \frac{\partial g}{\partial X_i} \Delta X_i + \frac{\partial g}{\partial x_i} \Delta x_i \right\} = 0, \quad (8)$$

and we can easily obtain a formula for $V_\theta = \text{Var}(\Delta \theta)$:

$$V_\theta = \sum_i E_i P E_i' + \sum_i F_i Q F_i'. \quad (9)$$

where $E_i = \left(\frac{\partial g}{\partial \theta}\right)^{-1} \frac{\partial g}{\partial X_i}$, $F_i = \left(\frac{\partial g}{\partial \theta}\right)^{-1} \frac{\partial g}{\partial x_i}$. The formulae for $\text{Var}(X_0)$, $\text{Cov}(\theta, X_0)$, etc. can also be derived in a similar way, though here we omit the details.

5 EVALUATION

In this section we describe some numerical simulations used to examine the numerical solution described in §3 and the error analysis described in §4.

5.1 Simulation Settings

The setting of the simulation was as shown in Fig. 5.

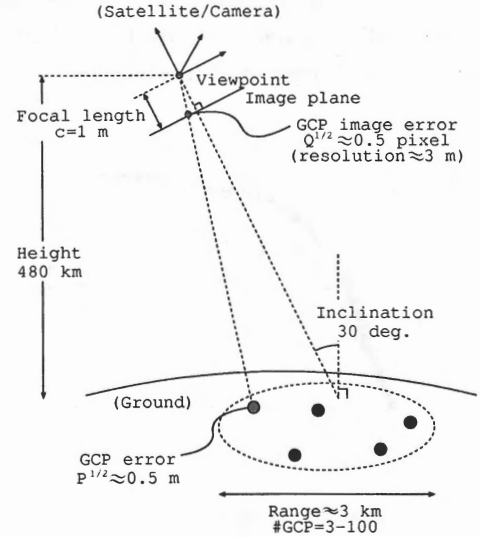


Fig. 5: Simulation settings.

In each simulation we first generated a set of imitation GCP data $\{(X_i, x_i) : i = 1, 2, \dots\}$ according to the setting and then made from them the list of solutions L in the way described in §3. We set the maximum size of L to be 5, and the GCPs were distributed randomly within a radius of about 3km. We ran 100 simulations to calculate statistics for each number of GCPs.

5.2 Stability of Numerical Solution

Table 1 lists, for various numbers of GCPs, the number of times (in 100 simulations) that the desired solution was Found/Chosen out of the list of solutions L .

GCPs	3	4	5	10	20	50	100
Found	100	100	100	100	100	100	100
Chosen	60	95	100	100	100	100	100

Table 1: Stability of numerical solution.

The desired solution was always found regardless of n , and it was correctly chosen when $n \geq 5$. When the techniques described in §3 were not used, the desired solution was less frequently Found/Chosen.

5.3 Validity of Variance Formulae

As measures of the validity of the variance formulae in §4, we use the statistics α_θ and α_{X_0} defined below. Let θ be the true value of camera angle, $\hat{\theta}$ its estimated value, and \hat{V}_θ the estimated variance of $\hat{\theta}$ calculated by (9). Define $\alpha_\theta = (\hat{\theta} - \theta)' \hat{V}_\theta^{-1} (\hat{\theta} - \theta)$. Define X_0 , \hat{X}_0 , \hat{V}_{X_0} , and α_{X_0} in a similar way. If the variance formulae are valid, α_θ and α_{X_0} will both obey the χ^2 distribution with 3 degrees of freedom.

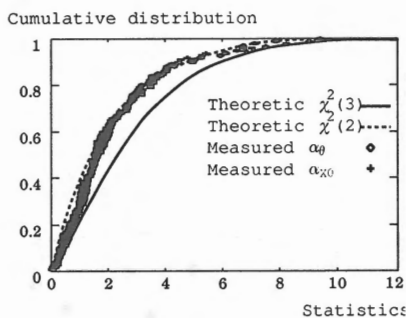


Fig. 6: Distributions of statistics α_* , χ^2 .

Fig. 6 shows the distributions of α_θ , α_{X_0} actually measured by the numerical simulation when #GCP=5, together with the theoretic χ^2 distributions. The distributions of α_θ , α_{X_0} fit well into χ^2 (but with a degree of freedom 2, rather than 3).

6 CONCLUSIONS

We derived simplified equation of space resection

(§2). The proposed numerical solution (§3) enables us to find the global minimum of the square error function stably and efficiently, something that has conventionally been rather difficult. We also derived and showed the validity of variance formulae (§4) that enable us to guarantee or predict the precision of the estimators. Thus we have developed a practical system of space resection (at least in cases where there is no lens distortion).

We have also shown theoretically that these results are almost the best possible in the situation considered. The techniques of nonlinear optimization in §3 – the absolute Newton method and others – are applicable to a wide range of nonlinear optimization problems.

References

- [Fu et al., 1987] Fu, K.S., Gonzalez, R.C., and Lee, C.S.G., 1987. Robotics: Control, Sensing, Vision, and Intelligence, McGraw-Hill, New York.
- [Kahaner et al., 1989] Kahaner, D., Moler, C., and Nash, S., 1989. Numerical Methods and Software, Prentice-Hall.
- [Levy et al., 1985] Levy, A.V., Montalvo, A., 1985. The Tunneling Algorithm for the Global Minimization of Functions, SIAM Journal on Scientific and Statistical Computing, Vol. 6.
- [Milnor, 1963] Milnor, J., 1963. Morse Theory. Ann. of Math. Studies, Princeton.
- [Wilks, 1962] Wilks, S.S., 1962. Mathematical Statistics, John Wiley.

APPENDIX

A.1 Notations

Most notations used in this paper are listed in Table 2 and also illustrated in Fig. 1. $SO(3)$ is a special orthogonal group and T^3 is a torus. “ $'$ ” stands for matrix transposition. In general, a notation with superscripts such as B^{kl} represents the component of the matrix or vector B .

Some of these notations may need more concrete descriptions. They are

Notation	Meaning	Coordinate System	Value
X_0	Camera position	Ground	R^3
X_i	i -th GCP	Ground	R^3
c	Focal length	Camera	$R(> 0)$
x_i	Image of i -th GCP	Camera	R^3
$A_i = A(x_i)$	A basis of orthogonal complement of $\langle x_i \rangle$ (actually, $\text{rank}(A_i) = 2$ and $A_i' \cdot x_i = 0$)	Camera	3×2 matrix
$R = R(\theta)$	Camera orientation	(Ground)	$SO(3)$
θ	Camera orientation parameter	(Ground)	$T^3 = (R/2\pi Z)^3$
P	Variance of measurement error of GCPs	Ground	3×3 matrix
Q	Variance of measurement error of GCP images	Ground	2×2 matrix
S_i	Weight of i -th GCP	—	2×2 matrix
r	Typical distance between camera and GCPs	Ground	$R(> 0)$
$\langle F \rangle$	Vector space spanned by (columns of) matrix F	—	—

Table 2: List of notation.

$$\begin{aligned}
R(\theta) &= \begin{pmatrix} 1 & 0 & 0 \\ 0 & \cos \theta_1 & -\sin \theta_1 \\ 0 & \sin \theta_1 & \cos \theta_1 \end{pmatrix} \times \\
&\quad \begin{pmatrix} \cos \theta_2 & 0 & \sin \theta_2 \\ 0 & 1 & 0 \\ -\sin \theta_2 & 0 & \cos \theta_2 \end{pmatrix} \times \\
&\quad \begin{pmatrix} \cos \theta_3 & -\sin \theta_3 & 0 \\ \sin \theta_3 & \cos \theta_3 & 0 \\ 0 & 0 & 1 \end{pmatrix} \\
x_i &= \begin{pmatrix} x_i^1 & x_i^2 & -c \end{pmatrix}' \\
A_i &= \begin{pmatrix} c & 0 & x_i^1 \\ 0 & c & x_i^2 \end{pmatrix}'
\end{aligned}$$

A.2 Supplementary Arguments Related to the Numerical Solution

A.2.1 Initial Value Setting: We describe how to set the initial value θ_0 in the ‘‘Initial Value Setting’’ stage of the numerical solution (Fig. 3). Let $L = \{\theta_1, \dots, \theta_k\}$ be the list of solutions of (5) already found, $k = \#L$ be the size of the list (with the initial values $\emptyset, 0$ respectively), $h = h(\theta)$ be the position function (6), and T_1, T_2 be transformations like those described in Fig. 7. Then the procedure is this:

1. $\theta_0 := \begin{cases} T_1(\theta_k) & \text{if } k > 0 \\ \text{given value (e.g. } 0) & \text{if } k = 0 \end{cases}$
2. If height of $h(\theta_0) < 0$ then $\theta_0 := T_2(\theta_0)$
3. If $\exists \theta_i \in L$ near θ_0 then $\theta_0 := \text{given value}$

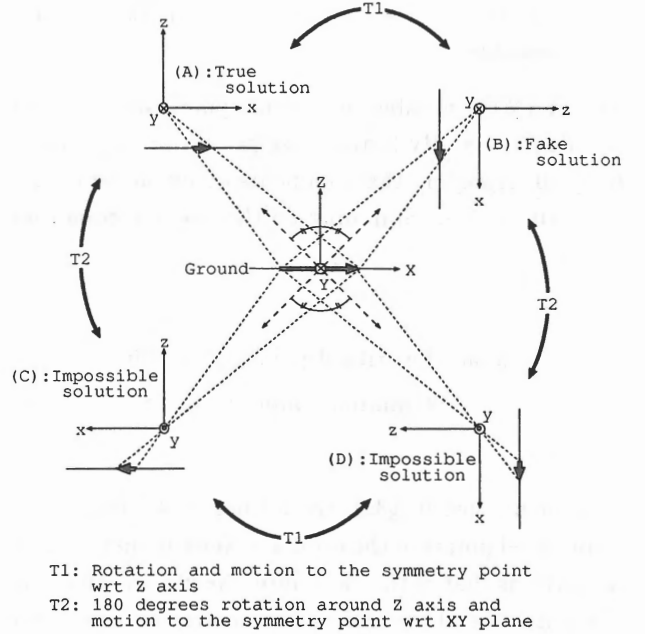


Fig. 7: Four almost equivalent camera locations.

The above procedure is supported by the following geometrical considerations. Since the visual angle of the satellite camera is fairly small, a central projection differs from the orthogonal projection only by a scale factor. Thus if the GCPs are distributed in a horizontal plane, we get similar pictures from four viewpoints (A)-(D) like those in Fig. 7, and correspondingly the square-error function (3) has four minimal points.

With the above procedure, we can find possible solutions (A), (B) (step (1)) and omit searching for phys-

ically impossible solutions (C), (D) (step (2)).

A.2.2 Number of Solutions – Background of Absolute Newton Method: Below we estimate the number of solutions of (5), $\nabla e = 0$, by some topological (Morse theoretic [Milnor, 1963]) considerations.

As in §3 we regard e as a function on the space of camera angle T^3 . Let m_i be the number of (non-degenerate) critical points of e with index i and let $B_i = \dim H^i(T^3)$ be the i -th Betti number of T^3 . Then the following holds (rigorously, except for the following item 1):

1. As a function on $SO(3)$, (3) has $m_0 \approx 4$ minimal points (§A.2.1).
2. The mapping degree of $R : T^3 \rightarrow SO(3)$ is 2.
3. The Betti numbers of T^3 are $B_0 = B_3 = 1, B_1 = B_2 = 3$.
4. $\sum_i (-1)^{k-i} m_i \geq \sum_i (-1)^{k-i} B_i$ for $\forall k$ (Morse's inequality).

By 1 and 2 the number of minimal points of e is about $m_0 \cdot \deg R = 8$. By 3 and 4 we get $m_1 \geq m_0 + B_1 - B_0 \geq 10$. Applying the arguments above to $-e$ we get $m_2 \geq 10, m_3 \geq 8$. Summing up the above inequalities we get

$$\begin{aligned} \#(\text{all the critical points}) &\geq 36 \\ \#(\text{minimal points}) &\approx 8 \end{aligned}$$

As mentioned in §3.3, the former is the number of stable fixed points of the ordinary Newton method and the latter is that of the "absolute" Newton method. In this sense the above estimation shows the advantage of the "absolute" Newton method over the ordinary one.

A.2.3 Numerical Differentiation: Numerical solution (§3.2) and error estimation (§4) require a number of partial derivatives. To calculate the partial derivatives, we wrote a program implementing the following numerical differentiation:

$$\begin{aligned} \frac{\partial f}{\partial x_i} &= \frac{1}{\Delta} \sum_{k=1, \dots, 4} w_k^1 f_i^k \\ \frac{\partial^2 f}{\partial x_i \partial x_j} &= \begin{cases} \frac{1}{\Delta^2} \sum_{k=1, \dots, 4} w_k^d f_i^k & \text{if } i = j \\ \frac{1}{\Delta^2} \sum_{k, l=1, \dots, 4} w_k^n w_l^n f_{ij}^{kl} & \text{otherwise} \end{cases} \end{aligned}$$

where $f_{ij}^{kl} = f(\dots x_i + \Delta \cdot d_k, \dots x_j + \Delta \cdot d_l, \dots)$, $f_i^k = f(\dots x_i + \Delta \cdot d_k, \dots)$; and the coefficients d_k, w_k^1, w_k^d, w_k^n are as in Table 3.

k	1	2	3	4
d_k	1	-1	1/2	-1/2
w_k^1	-1/6	1/6	1/8	-1/8
w_k^d	4/3	4/3	-4/3	-4/3
w_k^n	-1/36	1/36	8/36	-8/36

Table 3: Numerical differentiation coefficients.

One of the advantages of numerical differentiation is that we can save a great amount of labor and time in prototyping and development, since we do not need to write a program for each of a large number of partial derivatives. Numerical simulation shows that the numerical differentiation error amounts to less than 0.1% of the whole space resection error.

A.2.4 Efficiency of the Estimator: The least-square estimator $\hat{\theta}$, the global minimum of the square error function (3), is the best possible in the sense that it is unbiased (i.e., the expected value is 0) and efficient (i.e., the variance is equal to the Cramér-Rao's lower bound). To show this, we assume below that the errors of the observables are independent 0 mean Gaussian and that the second-order terms are negligible. We also assume appropriate regularity.

The unbiasedness of $\hat{\theta}$ is clear from (8) and the unbiasedness of each observed value.

It is well known that the maximum likelihood estimator is asymptotically efficient [Wilks, 1962], and it is easily seen to be actually efficient in the linear Gaussian case. Thus for the efficiency, it is enough to show that $\hat{\theta}$ is the maximum likelihood estimator.

The variance V_i of the error of the collinearity condition (1) is easily found to be

$$V_i = (RA_i)' P (RA_i) + \{e_3'(X_i - X_0)\}^2 Q$$

In a situation typical in satellite image processing (the visual angle is small; P, Q are isotropic; etc), the above V_i can be regarded as a constant " $c^2 \cdot P + r^2 \cdot Q$ " near the solution, which is a scalar independent of i . Thus if we simply set $S_i =$ unit matrix in (2) as we did in §2, the square-error function (3) differs from the logarithmic likelihood function only by a constant. This implies the efficiency of $\hat{\theta}$. \square